MORPHOLOGICAL EVOLUTION OF CONTINUOUS FIBER NETWORKS DURING ADDITIVE MANUFACTURING

Peters, N.[1*], Elderfield, N.[1], Sudak, L.J.[1] and Wong, J.C.H[1]

[1] Department of Mechanical and Manufacturing Engineering, University of Calgary, Calgary, Canada

* Corresponding author (klaas.peters@ucalgary.ca)

Keywords: *fused filament fabrication, discrete in-situ consolidation, warping*

ABSTRACT

Continuous fiber-reinforced thermoplastic composites manufactured via material extrusion (MEX) additive manufacturing processes have typically suffered from poor interlaminar bonding and high void contents due to incomplete consolidation combined with decompaction of the fiber network during deposition. To counter this, a discrete in-situ consolidation (DISC) process that uses a flat heated tool to apply local consolidation pressure along the length of each deposited bead was previously introduced. It has been observed that DISC significantly changes the fiber network morphology from the initially deposited material, but the morphological evolution is not yet well understood. Here, micro computed tomography (μCT) and optical microscopy are used to examine the progression of fiber redistribution during consolidation. μCT reveals that significant fiber rearrangement occurs in the bead beneath the consolidation tool resulting in a thinning and spreading of the bead, squeeze-out of the thermoplastic matrix, and transverse warpage of the bead. A process parameter study is performed that demonstrates the effects of consolidation force, temperature, and speed and correlates them to bead thickness, bead width, matrix squeeze-out, and transverse bead warpage.

1   INTRODUCTION

Producing continuous fiber-reinforced thermoplastic composites via additive manufacturing presents unique opportunities for design optimization due to its ability to precisely control fiber orientation and placement through a part using computer numerical control. However, material extrusion (MEX) additive manufacturing processes, e.g., fused filament fabrication (FFF), still require post-consolidation such as compression molding or vacuum bagging to reduce void contents to an industry-acceptable level. The poor consolidation results from low compaction pressure during material deposition which leads to significant inter-bead porosity. Additionally, deconsolidation of the fiber network due to stored strain energy can further exacerbate void growth. To counter this, a discrete in-situ consolidation (DISC) process was previously introduced wherein a flat heated tool applies local consolidation pressure along the length of each bead [1]. While it has been observed that DISC significantly changes fiber network morphology from the initially deposited material, the degree and mechanism of morphology changes, and their relation to consolidation parameters have not been investigated. Here, micro computed tomography (μCT) is used to examine the mechanisms of fiber redistribution during consolidation, and optical microscopy is used in a full factorial study to determine the effects of consolidation force, temperature, and speed on bead thickness and width. This analysis revealed the additional phenomena of matrix squeeze-out and transverse warpage in consolidated beads which were also examined.
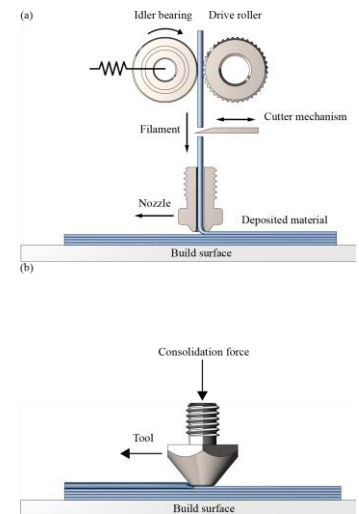

Figure 1: (a) FFF and (b) DISC working diagrams.

2 MATERIALS AND METHODS

2.1 Sample preparation

Samples were manufactured using a 3K carbon fiber-reinforced polyamide 12 (PA12) 3D printer filament (Filaprem 11590, Suprem SA, Yverdon-les-Bains, Switzerland) with a 55.0% fiber volume fraction and a cross-sectional area of 0.191 mm^2 [2]. This filament was found to have a melting temperature T_m of 177 °C from differential scanning calorimetry (DSC) using a Mettler Toledo DSC 3. The fibers had an average diameter of 6.7±0.1 µm. A full factorial experiment was performed to identify the effects of consolidation speed, temperature, and force on the morphology of beads with parameters described in Table 1. Each sample was deposited on an unheated glass bed with a nozzle temperature of r280 C, deposition height of 0.30 mm and speed of 300 mm/min (Figure 1a). To consolidate the samples, a 4 mm diameter flat-bottomed tool was run along the length of the deposited bead, remelting the matrix and compacting the material (Figure 1b). 375 mm long samples were embedded in a cold-mounting epoxy, cross-sectioned 6 times along their length, and polished. Bright-field micrographs of the sections were captured using an optical microscope (DM6000 M, Leica Microsystems, Wetzlar, Germany) with a 10 MP camera (MC190 HD, Leica Microsystems).

Table 1: Consolidation parameters used in the full factorial experiment.

Parameter	Values
Force (N)	5, 10, 15, 20, 25
Temperature (°C)	240, 260, 280, 300
Speed (mm/min)	25, 50, 100, 200, 400

2.2 Cross-sectional morphology characterization

Fiber centerpoint coordinate data from each cross-sectional micrograph (Figure 2a) were extracted using a script developed in ImageJ, an open-source image editor. To enable the use of a brightness maxima search algorithm, the central pixels of each fiber needed to be brightest. In original form, a brightness intensity plot (Figure 2b) shows fibers as plateaus without a distinct central peak. Application of a convolution kernel (Figure 2c) resulted in a brightness maximum at the center of each fiber (Figure 2d). This enabled automated extraction of centerpoint locations (Figure 2e).
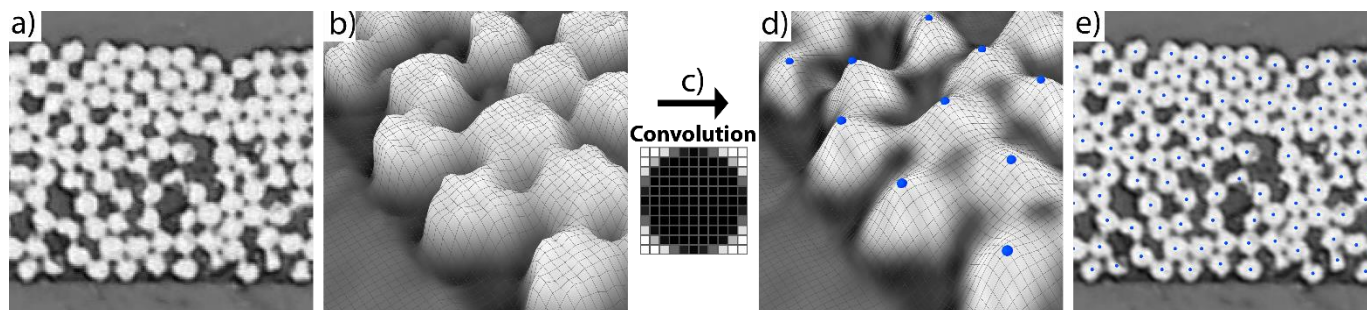

Figure 2: Workflow for automated determination of fiber centerpoints. (a) and (b) show pre-convolution images and pixel brightness intensity surfaces. A convolution kernel (c) is applied, then (d) and (e) show post-convolution pixel brightness intensity surfaces and resultant centerpoints.

For each micrograph, the computer-aided design software Rhinoceros (Rhinoceros 3D, Robert McNeel & Associates, Seattle, WA) was used to generate a mesh from fiber centerpoints via Delaunay triangulation [3]. To obtain the bulk fiber network geometry, the mesh was filtered by removing mesh elements with edge lengths exceeding a value of

18 µm. Cross-sectional area, bead width (W), and bead thickness (t) were measured from the fiber network mesh (Figure 3). A circle-of-best-fit was performed along the bottom surface of the mesh to measure the radius (R) and curvature (R^{-1}) of transverse warpage.

Figure 3: Geometrical Measurements taken from bead cross-sections.

Matrix squeeze-out (S) is herein defined as the volume fraction of matrix that has migrated out of the bulk fiber network during processing. It can be calculated as a function of packing efficiency in the bulk fiber network (v_c), and the initial feedstock fiber volume fraction (v_i):

$$S = \frac{v_c - v_i}{v_c(1 - v_i)} \tag{1}$$

2.3 Micro computed tomography

Micro computed tomography (Xradia 620 Versa, Carl Zeiss AG, Oberkochen, Baden-Württemberg, Germany) was conducted on a sample having undergone partial consolidation. A sample bead was deposited, then consolidated with the consolidation head rapidly retracted midway along the sample. A resolution of 1.78 µm/voxel was used.

3 RESULTS AND DISCUSSION

3.1 Micro computed tomography

A top-down view of the µCT scan showing the transition region between the as-deposited and consolidated bead is shown in Figure 4a. The as-deposited, unconsolidated bead (Figure 4b) has a thick and narrow cross-section, with some fibers separated from the primary bulk of the bead. Due to its non-rectangular profile, the bead will exhibit poor packing efficiency with adjacent beads resulting in inter-bead porosity. Furthermore, due to the lack of compaction pressure during deposition, the bottom surface does not conform to the profile of the underlying substate. As seen in previous works [1], this has significant implications in multi-layer samples, where interlaminar shear strength is compromised.
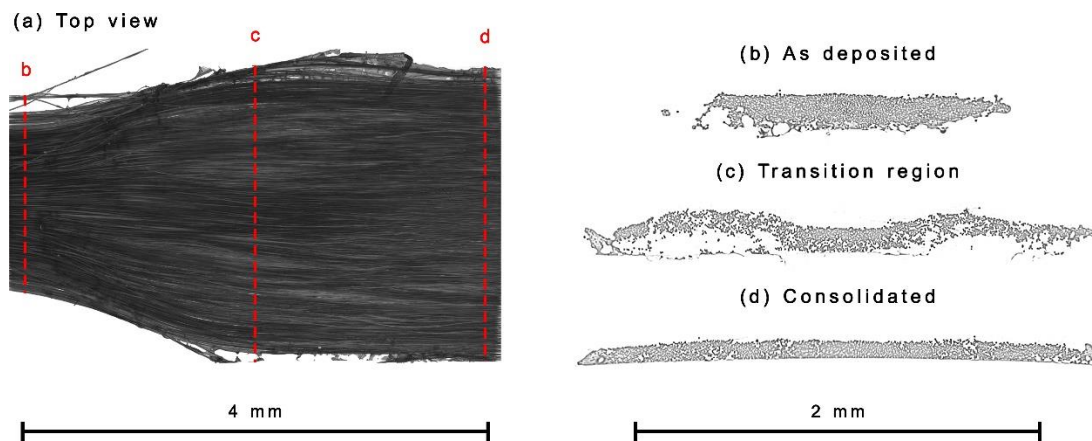

Figure 4: µCT images of a bead which has undergone partial consolidation: (a) Top view of the complete sample. (b-d) Stages of cross-sectional fiber and matrix rearrangement during the consolidation process.

As consolidation proceeds, several distinct mechanical phenomena are observed (Figure 4c). The center of the cross-section remains in place while fibers farther from the central axis spread outwards. By tracing fibers in the µCT scan using a fiber centerpoints (section 2.2), it is observed that the vertical displacement of fibers and all of the fiber

spreading occurs under the consolidation tool (Figure 5). The vertical displacement seen is believed to have occurred upon retraction of the consolidation tool due to stored strain energy. The final consolidated profile (Figure 4d) is notably thinner and more spread than the as-deposited profile. It exhibits a smooth bottom profile, indicating that it has fully conformed to the substrate. A slight transverse warpage has developed, possibly due to mechanical and thermal stresses.
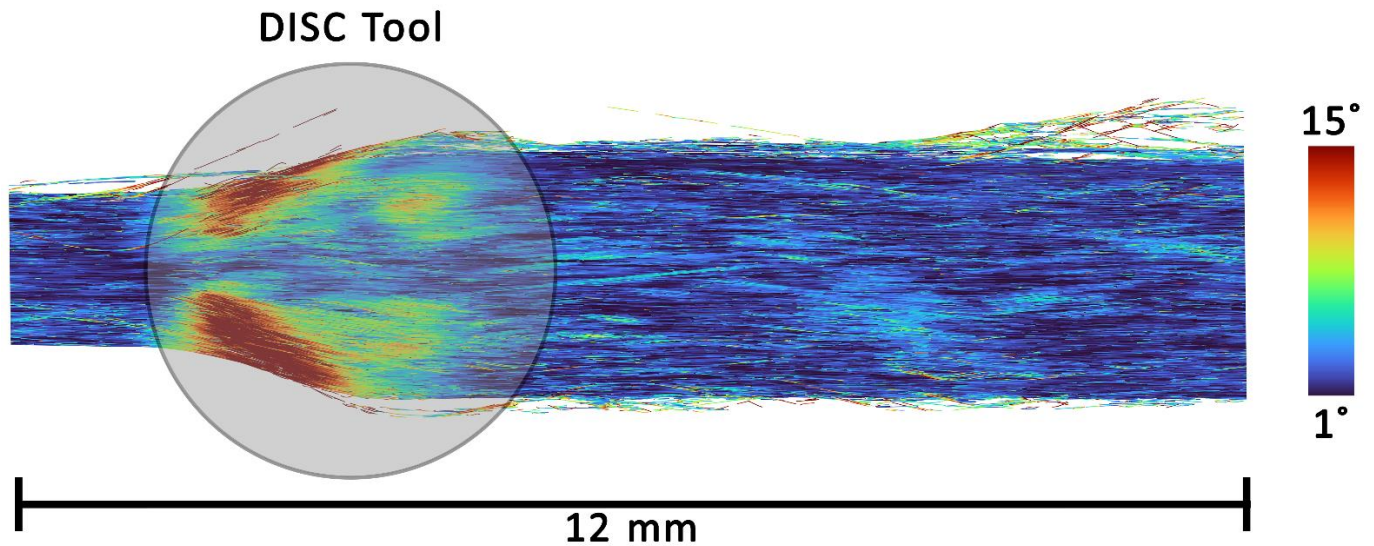

Figure 5: Fiber-traced µCT scan of partially consolidated sample; fibers are coloured according to total angle with respect to the horizontal axis. As consolidation proceeds, the DISC tool moves to the left, spreading the bead beneath it.

3.2 Effect of processing parameters on final bead dimensions

The thickness and widths of all consolidated beads were measured to determine their relationship to processing parameters. A minimum average thickness of 71 µm was found to occur at a force of 20 N, temperature of 300 °C, and speed of 50 mm/min. A maximum average thickness of 146 µm occurred at a force of 5 N, temperature of 240 °C, and speed of 400 mm/min. The thinnest samples resulted from a combination of high force, high temperature, and low speed, while the opposite produced the thickest samples (Figure 6). The effects of processing parameters on thickness are shown in Figure 7. Temperature and force exhibit negative correlations to thickness, while with speed, it is positive.
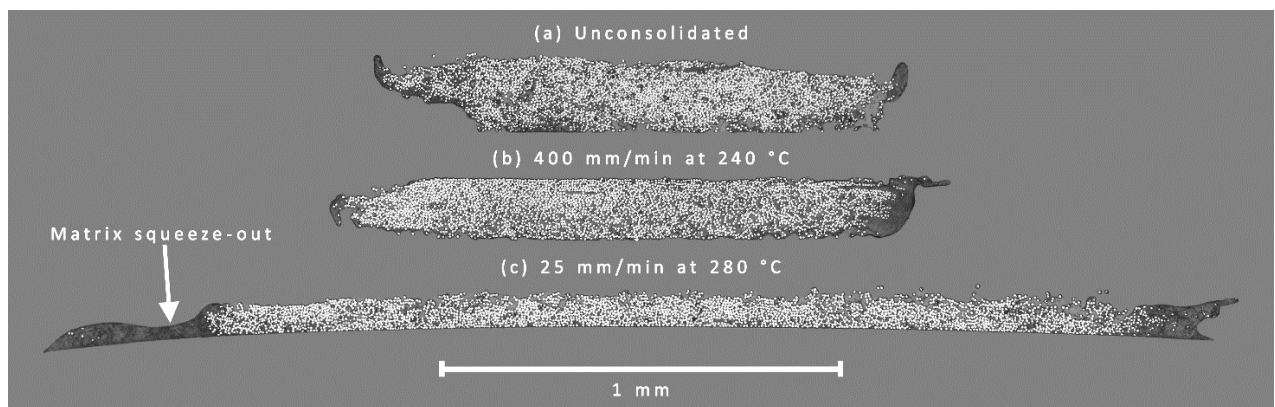

Figure 6: Transverse optical micrographs of processed beads: (a) As-deposited. (b) Minimally consolidated. (c) High degree of consolidation.
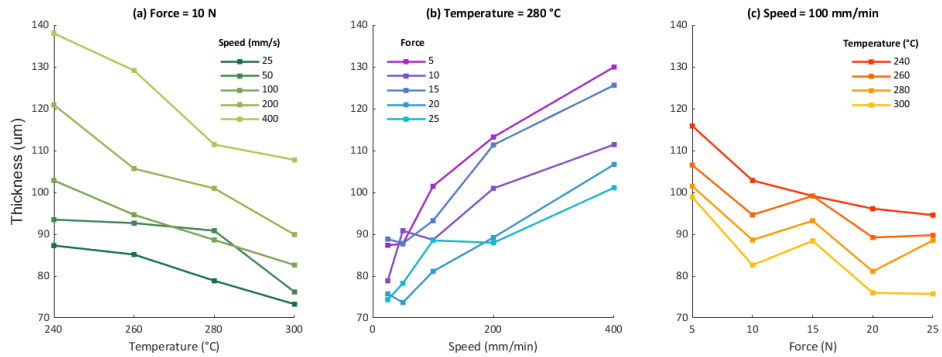
Figure 7: Thickness of consolidated samples with respect to parameters (a) temperature, (b) speed, and (c) force.

These correlations hold inversely for bead width as seen in Figure 8. These relationships are intuitive given the mechanics of consolidation. As temperature increases, viscosity of the PA12 matrix has been shown to exhibit an exponential relationship to the inverse of temperature [4]. Thus, as matrix temperature increases, resistance to flow of the matrix decreases and fibers can move more freely. Increased time under consolidation from a slower consolidation speed allows more time for this matrix and fiber rearrangement, with higher applied pressure increasing load on the fibers and thus also increasing the degree of fiber rearrangement.
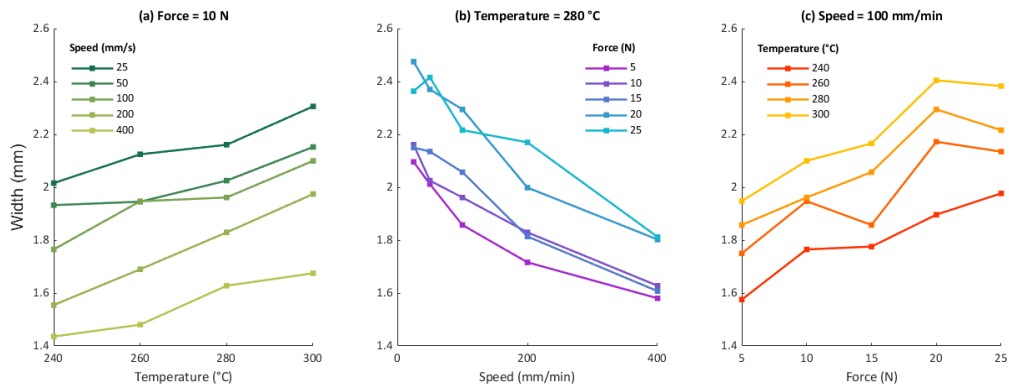

Figure 8: Width of consolidated samples with respect to parameters (a) temperature, (b) speed, and (c) force.

3.3 Matrix squeeze-out and transverse warpage
The level of visible matrix squeeze-out is marginal in as-deposited beads (Figure 6a) but increases significantly under consolidation. Matrix squeeze-out appears only to have a strong relation to processing speed (Figure 9a).
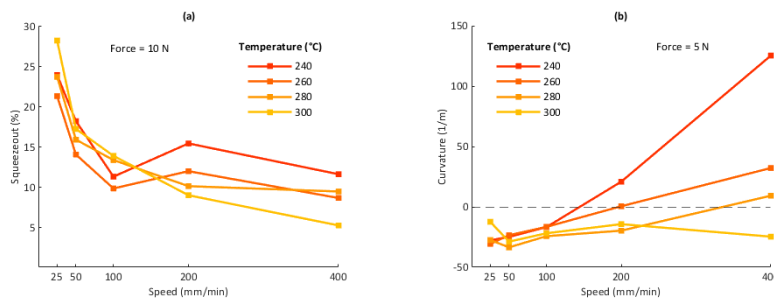

Figure 9: (a) Matrix squeeze-out and (b) transverse bead warpage as a function of consolidation speed. Positive curvature indicates edges of the bead warp upwards.

5

Previous studies on consolidation of fiber bundles within a matrix material reveals that during initial compaction, the matrix bears the majority of pressure from consolidation [5]. However, as matrix flows out transversely from the primary fiber bundle, pressure in this matrix rapidly drops as the consolidation load is taken up by increased fiber-on-fiber contact brought on by compaction. As such, force ceases to be a variable affecting matrix squeezeout shortly after consolidation onset. However, by slowing down consolidation speed, the matrix spends more time elevated above melting temperature, allowing for increased flow out of the bulk fiber network.

Transverse warpage of beads was consistently noted across many samples, particularly those which had undergone slower consolidation speeds (Figure 9b). As the processing speeds are lowered, the warpage curvature tends to converge towards a negative value, indicating warping of the edges of the bead downwards. High positive warpage indicates that the sample has not undergone significant rearrangement from the as-deposited profile (Figure 6b). This warpage is possibly a result of residual compressive stresses held in the fiber network upon solidification of the matrix. Alternatively, it could be due to thermal gradients in the cooling thermoplastic matrix.

4 CONCLUSIONS

It was found that during DISC, fibers exhibit transverse motion under the consolidation tool as the primary mechanism for fiber spreading. Within the parameter range studied, thickness showed a 51% reduction from the thickest to thinnest sample, exhibiting strong correlations to force, temperature, and speed. Matrix squeeze-out and transverse bead warpage were observed to be strongly correlated to processing speed. Future work will focus on the mechanisms responsible for this warpage, and its effect on part-level warpage in thin (1-3 layer) composite sheets.

5 ACKNOWLEDGEMENTS

6 REFERENCES

[1] N. Elderfield and J. C. H. Wong, 'Discrete in-situ consolidation of additively manufactured continuous fiber-reinforced polymer composites', *Composites Part A: Applied Science and Manufacturing*, vol. 171, p. 107562, Aug. 2023, doi: 10.1016/j.compositesa.2023.107562.

[2] N. Elderfield and J. C. H. Wong, 'The effects of over-extrusion on the in-situ consolidation of additively manufactured composites', *ICCM 23*, pp. 1–12, Jul. 2023.

[3] A. Bowyer, 'Computing Dirichlet tessellations*', *The Computer Journal*, vol. 24, no. 2, pp. 162–166, Jan. 1981, doi: 10.1093/comjnl/24.2.162.

[4] N. Bernet, V. Michaud, P. E. Bourban, and J. A. E. Manson, 'An Impregnation Model for the Consolidation of Thermoplastic Composites Made from Commingled Yarns', *Journal of Composite Materials*, vol. 33, no. 8, pp. 751–772, Apr. 1999, doi: 10.1177/002199839903300806.

[5] T. G. Gutowski, Z. Cai, S. Bauer, D. Boucher, J. Kingery, and S. Wineman, 'Consolidation Experiments for Laminate Composites', *Journal of Composite Materials*, vol. 21, no. 7, pp. 650–669, Jul. 1987, doi: 10.1177/002199838702100705.